Ignition and combustion study of premixed ammonia using GDI pilot injection in CI engine

Førby, Niels; Thomsen, Thomas B.; Cordtz, Rasmus F.; Bræstrup, Frantz; Schramm, Jesper

Published in:
Fuel

Link to article, DOI:
10.1016/j.fuel.2022.125768

Publication date:
2022

Document Version
Publisher's PDF, also known as Version of record

Fuel 331 (2023) 125768

Contents lists available at ScienceDirect

Fuel

journal homepage: www.elsevier.com/locate/fuel

Full length article

Ignition and combustion study of premixed ammonia using GDI pilot injection in CI engine

Niels Førby [a,*], Thomas B. Thomsen [b], Rasmus F. Cordtz [c], Frantz Bræstrup [d], Jesper Schramm [a]

[a] Technical University of Denmark, Kgs. Lyngby, Denmark
[b] Strandmøllen, Klampenborg, Denmark
[c] Danish Technological Institute, Høje Taastrup, Denmark
[d] FORCE Technology, Department of Clean Air Technologies, Brøndby, Denmark

ARTICLE INFO

Dataset link: https://doi.org/10.11583/DTU.20555586.v2

Keywords:
Combustion
Ammonia combustion
CI-engine

ABSTRACT

In this study ignition of premixed ammonia was tested using a compression-ignited (CI) pilot fuel. *n-heptane* (C_7H_{16}) was used as pilot fuel, injected with a GDI injector, enabling very small pilot fuel injections. With this setup, the engine was run using up to 98.5 % energy from ammonia – higher than seen in other CI-engine studies with ammonia at the time of writing. The ammonia energy contribution was varied 80–98.5 %, while keeping the total λ-value constant. An important result observed was an increase in combustion efficiency from 81%–90% with higher ammonia energy due to a lower local λ-value of the ammonia–air mixture, indicating that for ammonia-ignition an easily ignitable ammonia–air mixture is preferable compared to a strong pilot injection. Lean ammonia–air mixtures showed a gap in heat release between the pilot and ammonia combustion phases, which lowered the combustion efficiency. Increased ammonia energy led to reduced ammonia-slip and N_2O-emissions and increased NO-emissions, and a lower CO-formation showed better pilot fuel oxidation.

1. Introduction

With the efforts to reduce greenhouse gas (GHG) emissions due to climate change, a focal point has been to replace fossil fuels with sustainable alternatives in the transport sector. The shipping industry is responsible for 2%–3% of the world's total GHG emissions [1], and the International Maritime Organization (IMO) has presented a goal to reduce the GHG by 50%, compared to 2008-levels, before 2050 [2]. Due to infeasibility of batteries and electric motors for long-range cargo-ships, sustainable fuels for internal combustion (IC) engines are investigated heavily at the moment, and ammonia (NH_3) is expected to see significant usage, because there are no CO_2-emissions from combustion of ammonia since it contains no carbon and can be made using hydrogen from electricity from renewable energy sources. Ammonia-usage in IC engines for marine purposes have been compared with fuel-cell usage, and IC engine use was concluded to perform better in terms of weight, volume, and cost [3]. However, before ammonia can be used as a main fuel on a large scale, research is needed to reduce both ammonia-slip, N_2O- and NO_x-emissions [4].

Spark-ignition (SI) engines have been shown to operate on ammonia for many years, with important work performed in the 1960's [5], and renewed interest has increased the research in recent years. Many SI-engine studies have used ammonia mixed with hydrogen for improved combustion stability due to the high flame speed of hydrogen [6–10]. Compared to conventional hydrocarbon combustion, using ammonia generally yields higher NO- and N_2O-emissions. N_2O has a global warming potential of 298 with climate–carbon feedback (265 without) [11], which makes it highly relevant for emission studies. It has been showed that fuel in crevice volumes was essential for nitrogen-based emissions [6]. Using ammonia as a fuel for compression-ignition (CI) engines remains a great challenge due to the high auto-ignition temperature of ammonia – more than 400 K higher than that of diesel at atmospheric conditions [12] – meaning that compression ratios higher than 35:1 are required for ammonia-only CI operation [13,14]. Other challenges for ammonia-operation is the high heat of vaporization, which significantly decreases in-cylinder temperature after injection [15]. Ammonia/air-mixtures also has a low flame speed, generally around 1/5 of methane/air mixtures [16], and hence large fuel slips can be observed using ammonia. As mentioned, hydrogen can be used to increase combustion speed. Due to these challenges, most studies regarding ammonia in CI engines are dual-fuel operation [12], often using diesel as a pilot fuel.

Reiter et al. [17] used a dual-fuel configuration with premixed ammonia and direct-injected diesel and varied the fuel contributions, first with 10%–45% energy contribution, then later [18] from 0%

* Corresponding author.
E-mail address: nilfor@dtu.dk (N. Førby).

https://doi.org/10.1016/j.fuel.2022.125768
Received 7 June 2022; Received in revised form 12 July 2022; Accepted 20 August 2022
Available online 3 September 2022

Nomenclature

$\dot{Q}$	Heat rate [J/CAD]
f	Residual gas fraction
p	Pressure [bar]
T	Temperature [°C]
V	Volume [m^3]

Greek Letters

η	Efficiency
γ	Specific heat capacity ratio, $\frac{c_p}{c_v}$
θ	Crank angle [° or CAD]

Subscripts

in	Intake (charge)
res	Residual gas

Acronyms

ATDC	After top dead center
BDC	Bottom dead center
CAD	Crank angle degree
CI	Compression ignition
DME	Dimethyl ether
EVO	Exhaust valve opening
FTIR	Fourier-transform infra-red
GDI	Gasoline direct injection
HCCI	Homogeneous charge compression ignition
HRR	Heat release rate
IVC	Intake valve closing
SACI	Spark-assisted compression ignition
SI	Spark ignition
SOC	Start of combustion
SOI	Start of injection
TDC	Top dead center

(diesel only) to around 80%. Among their key findings were that small amounts of ammonia energy yielded high brake-specific fuel consumption (BSFC) of ammonia due to very lean ammonia–air mixtures, while high ammonia energy showed high BSFC of diesel due to low temperatures. They also found that using small amounts of ammonia (e.g. 5%–20%) decreases the in-cylinder temperature resulting in decreased NO-emissions and increased and CO-emissions, compared to diesel-only. Larger amounts of ammonia energy (>50%) significantly increased NO emissions due to fuel-bound nitrogen. However, another study with port-injected aqueous ammonium and direct-injected diesel [19] showed the opposite trend of Reiter's results regarding NO-emissions: as ammonia-contribution was increased from 0% to 10% energy-contribution, the NO-emissions initially increased due to fuel-bound nitrogen, while larger amounts of ammonia (to 25%) showed a decrease in NO due to lower temperatures.

The vapor pressure of ammonia is similar to that of dimethyl ether (DME), which has a cetane-number higher than that of diesel, and this makes it attractive to improve the CI combustion properties of ammonia by mixing it with DME for a single-fuel CI-operation. Gross [20] found that, compared to 100% DME, the ammonia–DME mixture showed higher CO- and NO-emissions due to low temperatures and fuel-bound nitrogen, as well as higher ignition delay and cyclic variations. Another study [21], also employing a DME–ammonia mixture, with up to 60% ammonia, showed similar results. With 60% ammonia very early injection (−340 to −90 CAD ATDC) was necessary, which showed HCCI combustion with very abrupt heat release and high cyclic variations at low loads due to incomplete combustion. This also dramatically increased hydrocarbon- and CO-emissions.

A spark-assisted compression ignition (SACI) operation has recently been shown to run on neat ammonia [22]. SACI uses a spark for early partial combustion to increase the temperature, enabling compression-ignition for the main combustion. However, the two phases were not distinguished, and SI-like operation was obtained.

The presented CI-engine studies with ammonia generally uses up to 80% energy from ammonia, the rest from diesel – only a few results with higher levels are shown but are discarded due to high brake-specific fuel consumption [18]. In the longer perspective, a 100% sustainable fuel supply is desired. In this study, a dual-fuel concept with premixed ammonia and direct-injected n-heptane (C_7H_{16}) was implemented using a Bosch piezo-electric GDI injector for the direct-injected pilot fuel. This setup was chosen to investigate the possibility of running a CI-engine with higher ammonia-energy share than previously seen. The GDI injector allows small, quick injections with rapid atomization of the pilot fuel. The purpose of the study was to investigate the CI ignition and combustion processes with very high ammonia energy contributions.

n-heptane was chosen as pilot fuel due to its low viscosity and high cetane number. Some representative values of viscosity and cetane number for both diesel and n-heptane are shown in Table 1. Using a more viscous pilot fuel make very small injections difficult and yield larger spray droplets.

Table 1
Viscosity and cetane numbers of diesel and n-heptane for comparison.

	Diesel	n-heptane
Kinematic viscosity [mm^2/s]	3.8 [23]	0.57 [24,25]
Cetane number	>51[a] [26]	53–56[b] [27]

[a]Minimum cetane number and cetane index is 51 and 46, respectively, in EN 590 diesel fuel standard.
[b]Multiple values presented in the reference without specification of cetane number or index.

Table 2
Specifications for the BUKH DV 24 ME engine used.

Displacement volume	964 cm^3
Compression ratio	18
Effective compression ratio[a]	16.4
Max. power	17.6 kW
Bore	85 mm
Stroke	85 mm
Connecting rod length	160 mm
IVC[b]	−139 CAD
EVO[b]	126 CAD
Engine speed (this study)	1200 RPM

[a]*Effective* compression ratio is compression from IVC to TDC.
[b]IVC and EVO are presented in CAD ATDC.

2. Methods

Engine tests were performed using ammonia as primary fuel. The engine setup and the data processing will be briefly presented for both reproducibility and for discussion purposes.

2.1. Test engine set-up

The engine tests were performed with a BUKH DV 24 ME, a 2-cylinder compression-ignited diesel engine with a displacement volume of 964 cm^3, a compression ratio of 18 and a maximum power of 17.6 kW from the factory (see Table 2).

One cylinder was unchanged and thus operated normally with diesel, while the *test-cylinder* operated on ammonia as described in this

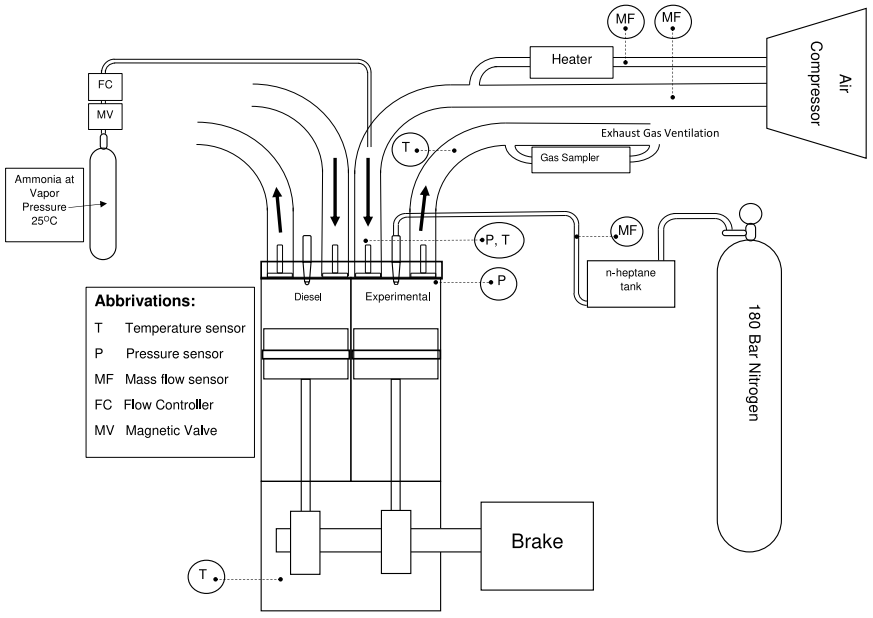

Fig. 1. Graphical illustration of test engine setup.

paper. Having a normally operating diesel-cylinder was useful for both motoring purposes, engine start-up and for altering fuel injection in the test cylinder without unstable operation.

Pressure in the test-cylinder was measured using a Kistler piezo-electric pressure pick-up with 10 pressure samples per CAD, controlled by a shaft encoder. The cylinder pressure was assumed to be equal to the intake pressure at IVC. The intake pressure was 1.22 ± 0.02 bar (measured for each test).

All tests were performed with an engine speed of 1200 RPM.

For the test cylinder, gaseous ammonia was aspirated into the intake manifold, and n-heptane was injected directly into the cylinder as a pilot fuel to ignite the ammonia–air mixture. n-heptane start of injection (SOI) was 20 CAD BTDC (except when stated otherwise). Earlier SOI – e.g. earlier than 50 CAD BTDC – would result in HCCI-like operation, which was not the purpose of these experiments. As the test engine was not equipped with a common rail system, the n-heptane was pressurized in a fuel tank by liquid nitrogen and driven to the injector, using the fuel pressure, through a mass flow controller. Due to limitations on the fuel tank, a max. pressure of 120 bars was used.

An illustration of the test engine setup is shown in Fig. 1.

2.1.1. Gas measurements

Emissions of gas species (CO, CO_2, NH_3, NO and N_2O) were measured using Fourier Transform Infra-Red spectroscopy (FTIR). The FTIR used for testing was a DX4000 from Gasmet Technologies Oy. Temperature of the sample gas was maintained at 180 °C through the FTIR sample system. A Dekati eDiluter Pro dilution system was applied in front of the FTIR to ensure sample gas concentrations to be within the measurement range of the analyzer. The diluter system was equipped with two dilution stages. The first dilution stage was heated to 180 °C and the second stage was kept at room temperatures. Dry pressurized air free of particle was used to dilute the sample gas below the dew point of water vapor. The dilution system includes a build-in compensation of possible fluctuations on the dilution factor due to variations of the sample gas pressure. The dilution factor was verified by applying a certified test gas from the inlet of the sample line to the analyzer and measure the concentration after dilution. A dilution factor of 30 was used in the test. A multi-component certified test gas covering the IR spectrum of the FTIR was used to calibrate the analyzer and verify that no leakage appeared in the sampling system. The test gas was applied before and after the test to verify and compensate for any detector drift.

Table 3
Specification of gas monitor.

Instrument	Model DX4000 from Gasmet^{TM}
Measuring principle	Fourier Transform Infra-red spectroscopy
Wavenumber range	900–4200 cm^{-1}
Sample cell	Multi-pass, fixed path length of 5.0 m
Temperature	180 °C
Measuring ranges of selected gas species	
CO	0–1000 ppm
CO_2	0–20 vol% 0–3000 ppm
NH_3	0–2000 ppm
NO	0–1000 ppm

Table 3 summarizes the specification of the FTIR instrument used in the test.

2.2. Data processing

For each measurement shown 50 full cycles were measured, and the average cycle was computed and used for data processing of each measurement. For curve smoothing, the cycle was filtered with a Savitzky–Golay filter [28]. The location of the top dead center (TDC) was assumed to be 0.5 CAD after the maximum pressure in the average motoring cycle due to heat loss and potential blow-by.

Pressure data, along with cylinder volume as a function of crank angle θ, was used to obtain the fuel-combustion heat release rate $\dot{Q}_{HR}$, through Eqs. (2.1) and (2.2):

$$\dot{Q}_{HR} = \dot{Q}_{HR,net} + \dot{Q}_{wall} \tag{2.1}$$

$$\dot{Q}_{HR,net} = \frac{\gamma}{\gamma - 1} \cdot p \cdot \frac{dV}{d\theta} + \frac{1}{\gamma - 1} \cdot V \cdot \frac{dp}{d\theta} \tag{2.2}$$

The *net* heat release rate is that calculated through pressure measurements (Eq. (2.2)). Since there is generally a heat loss from the gas

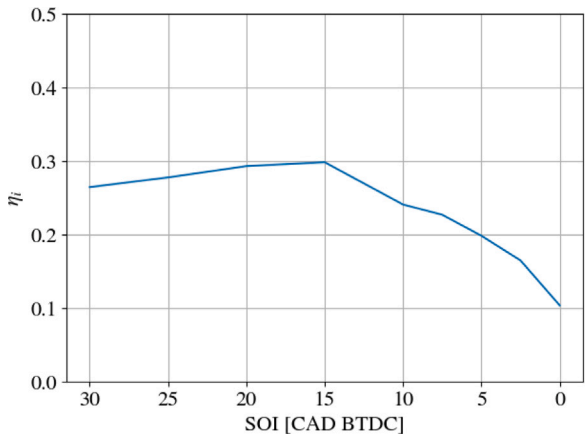

Fig. 2. Initial investigation of SOI. Conditions were 78% NH_3 energy contribution and global $\lambda = 1.15$.

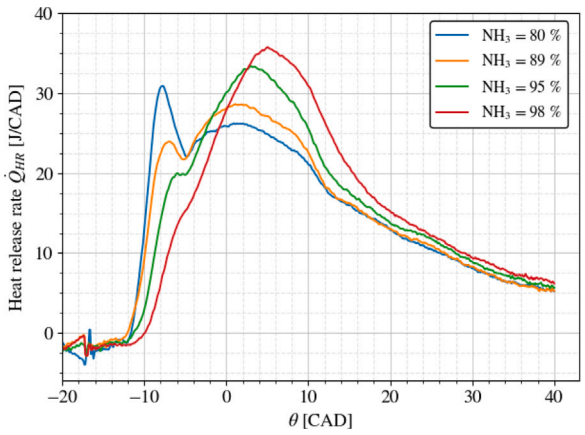

Fig. 3. Heat release rates for increasing ammonia energy, with a constant $\lambda = 1.1$.

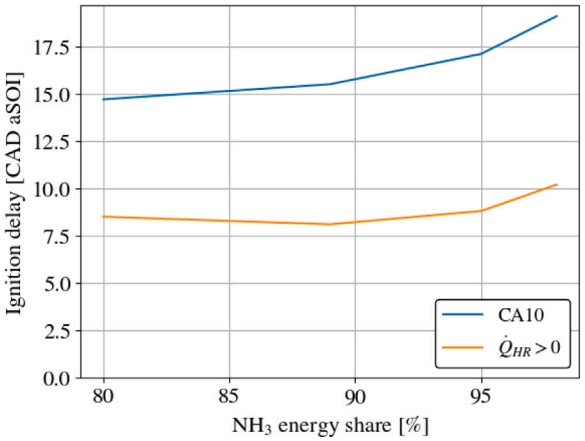

Fig. 4. Ignition delay, defined as SOC - SOI, for the results shown in Fig. 3. Both SOC for positive heat release rate and CA10 (10% fuel energy released) are shown.

to the walls, the *apparent* heat release rate (Eq. (2.1)) takes this into account. The wall heat transfer – $\dot{Q}_{wall}$ in Eq. (2.1) – was approximated using the Woschni correlation for the convective heat transfer coefficient [29]. For the bulk gas temperature used in the Woschni correlation, an ideal gas assumption was made, assuming a gas constant of $R = 287\ \frac{\mathrm{J}}{\mathrm{kg\,K}}$.

Dot-notation in Eqs. (2.1) and (2.2) () denotes units of J/CAD.

In order to take into account the residual gas in the cylinder, the temperature at IVC, T_{IVC} was approximated with Eqs. (2.3) and (2.4):

$$T_{IVC} = (1 - f) \cdot T_{in} + f \cdot T_{res} \tag{2.3}$$

$$\text{where} \quad T_{res} = T_{EVO} \left(\frac{p_{IVC}}{p_{EVO}} \right)^{\frac{\gamma-1}{\gamma}} \tag{2.4}$$

The residual gas fraction f was assumed to be 0.05 as it was expected to realistically be within the range 2%–8%. The sensitivity of this assumption is briefly analyzed in Section 3.1.1. Since T_{EVO} was needed to determine T_{IVC}, an iterative solving method was used for Eqs. (2.3) and (2.4). The indicated work was evaluated using the measured pressure data and volume function:

$$W_i = \int_{IVC}^{EVO} p\, dV \tag{2.5}$$

The combustion efficiency was defined as a fuel energy balance of the test cylinder:

$$\eta_c = 1 - \frac{\sum_i n_{i,out} \cdot \mathrm{LHV}_i}{\sum_j n_{j,in} \cdot \mathrm{LHV}_j} \tag{2.6}$$

Here n denotes the number of moles entering ($_{in}$) or exiting ($_{out}$) the test cylinder per cycle, LHV is the lower heating value and i is chemical species NH_3 and n-heptane while j is chemical species NH_3 and CO.

3. Results and discussion

Results from the engine tests will be presented in this section. An investigation on the ammonia energy share – i.e. the share of fuel energy supplied by ammonia – is presented in Section 3.1, followed by an analysis pertaining the intake temperature T_{in} in Section 3.2.

During initial tests the SOI was varied with a constant global $\lambda = 1.15$ and 78% ammonia energy contribution. The resulting indicated efficiencies are shown in Fig. 2. It was found that SOI at 20–15 CAD BTDC yielded best – and very similar – results, as later injection resulted in poor combustion efficiency due to the long combustion time for ammonia.

3.1. Variation in ammonia energy share

This section will present results from a variation of ammonia energy contribution from 80–98.5%.

Fig. 3 shows the heat release rate observed when increasing the ammonia energy-share from 80% to 98.5% with a constant $\lambda = 1.1$, by decreasing the pilot fuel flow and increasing the ammonia flow. It was chosen to keep the global λ and SOI constant, and consequently allow some variation in IMEP with changing energy contributions, because the purpose of this study was investigating the ignition and combustion processes. For engine concept feasibility the IMEP should be constant while using maximum brake torque SOI. The value of $\lambda = 1.1$ was chosen from initial studies showing high indicated efficiencies at this value.

SOI at 20 CAD BTDC was chosen from the results in Fig. 2. The ignition delays are shown in Fig. 4. Both the delays for positive heat release rate and CA10 (CAD for 10% of fuel energy released) are shown, both in CAD after SOI.

With 80% ammonia energy, a brief initial peak in heat release rate can be identified before a longer and slightly lower heat release rate takes place. The initial peak is most likely combustion of pilot fuel, while the longer and lower heat release rate is ammonia combustion. As the ammonia energy is increased – and the pilot fuel is correspondingly decreased – the initial peak decreases, as should be expected, and the ammonia combustion is seen to reach higher heat release rates. While the 80% NH_3 shows a relatively sustained heat release rate, the higher NH_3 amounts lead to higher peak HRR sustained for a shorter time.

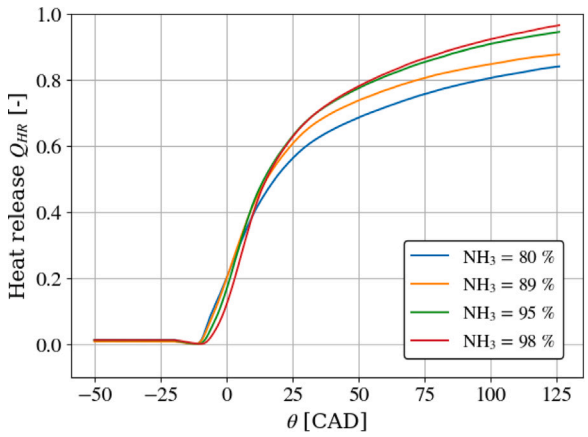

Fig. 5. Integrated heat release curves with increasing ammonia energy and constant $\lambda = 1.1$, normalized by the total fuel energy and shifted to begin combustion from 0 heat released.

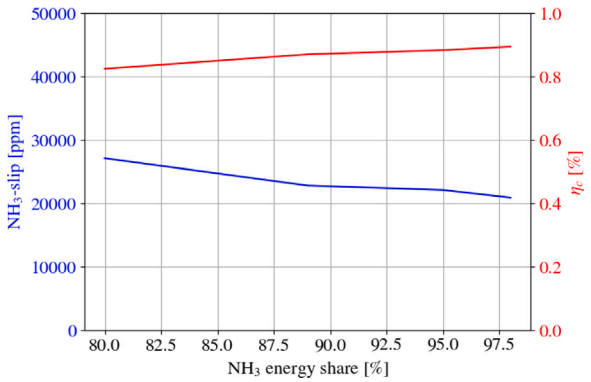

Fig. 6. Ammonia-slip and combustion efficiency η_c vs. ammonia energy share with constant $\lambda = 1.1$.

Table 4
Air excess ratio of the ammonia–air mix (λ_{NH_3}) and fuel energy (in J/cycle) for 4 levels of ammonia energy contribution levels.

NH$_3$ [%]	**80**	**89**	**95**	**98**
λ_{NH_3}	1.38	1.25	1.16	1.11
Fuel energy [J]	1290	1203	1190	1205

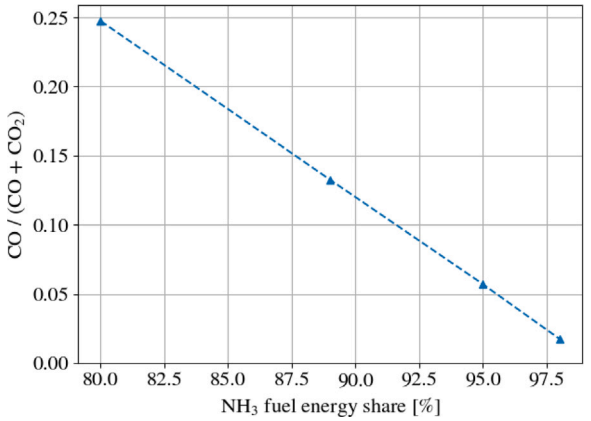

Fig. 7. CO-share of total carbon-based emissions (CO and CO_2): $\frac{CO}{CO+CO_2}$. The pilot fuel combustion is more rich with higher pilot fuel energy even though the total λ is unchanged.

This likely due to less ammonia fuel leading to a leaner ammonia–air mixture which inhibits the burning rate of the mixture. The pilot fuel combustion products may also act as inert gases during the ammonia combustion.

The initial investigation of SOI with 78% ammonia energy (Fig. 2) showed a trade-off between high compression work with early injection or low combustion efficiency with late injection, limiting the obtainable indicated efficiency. This can be identified in the gap between the pilot and ammonia combustion phases with 80% ammonia in Fig. 3. However, the 98% ammonia case shows a reduction of this trade-off since there is no gap between the fuel combustion phases and the maximum burning rate is higher. The potential for a large heat release close to TDC thus increases the obtainable indicated efficiency.

Fig. 4 shows that increased ammonia energy generally increases the ignition delay. This might be explained by the ammonia inhibiting the oxidation of the pilot fuel. As the ammonia-energy increases, the concentration of ammonia in the ammonia–air mixture increases. It is unclear to what extent the pilot fuel combustion products act as inert gases during the ammonia combustion.

The corresponding integrated heat releases are shown in Fig. 5, normalized by the total fuel energy and plotted to EVO. Note that these have been shifted to accommodate the heat for fuel vaporization. Important results from Fig. 5 are that more ammonia energy seem to yield more complete combustion, but all cases lead to incomplete combustion. A significant fuel amount is combusted very late in the expansion stroke, decreasing the generated work and hence indicated efficiency. Thus, to increase the indicated efficiency the combustion speed should be increased. The ammonia slip is shown in Fig. 6, where it is observed that the ammonia slip decreases when the amount of ammonia is increased, even in spite of the expected increase in ammonia in crevice volumes, clearly indicating an improved ammonia combustion efficiency. The combustion efficiency, η_c, also increases with higher ammonia energy share.

The increasing combustion efficiency with higher ammonia energy is believed by the authors to be a result of differences in local λ-values. A higher amount of energy from ammonia means that the local air-excess ratio of the ammonia–air mixture, λ_{NH_3}, decreases towards stoichiometric, making the mixture easier to ignite. Conversely, less energy from ammonia will leave more of the oxygen in the ammonia–air mixture for the pilot fuel, and the ammonia–air mixture will have a high local λ-value, making it less easily ignited and decreasing the flame speed. Table 4 shows the ammonia–air mixture λ-values, λ_{NH_3}, for the results in Figs. 3–6. The higher λ_{NH_3} from increased ammonia-energy leads to higher flame speeds, as the laminar flame speed is generally highest around $\phi = 1.1$, or $\lambda = 0.91$ [16,30].

Increasing the pilot fuel energy contribution will naturally increase the oxygen required for pilot fuel combustion while increasing the oxygen-concentration in the ammonia–air mixture. Fig. 7 shows that the CO-emissions, relative to the total carbon-based emissions (CO and CO_2), decrease with increasing ammonia-energy. The pilot fuel exhibits a similar but opposite issue of the ammonia–air mixture; more pilot fuel decreases the local λ-value at the spray to richer combustion, resulting in higher CO-formation. The substantial amounts of CO at 80%–89% ammonia-energy clearly shows a great disadvantage of the GDI injector: as a large amount of direct-injected pilot fuel is sprayed very quickly, a dense fuel 'cloud' is formed which is not easily oxidized while the temperature conditions allow fuel cracking, resulting in high CO-formation. Fig. 8 shows a graphical illustration of this expected cause of the poor combustion observed with 80%–89% ammonia-energy.

As mentioned earlier, it was chosen to keep the global λ constant in this analysis, and not the IMEP, to keep the combustion conditions comparable instead of the engine conditions. The resulting variation in IMEP, as well as Coefficient of Variation (CoV), are presented in Fig. 9. The IMEP increases slightly with the ammonia energy contribution, albeit this could be due to the increased combustion efficiency.

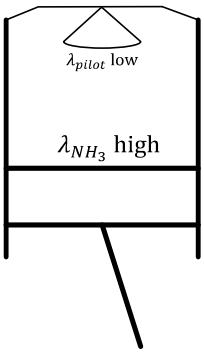

Fig. 8. Illustration of the expected explanation of the observed tendencies in Figs. 3, 5, 6 and 7 with a significant pilot fuel amount. A higher energy share from pilot fuel occupy more of the oxygen in the cylinder for pilot fuel combustion, and as a result, the ammonia–air mixture becomes lean while the pilot fuel combustion becomes rich.

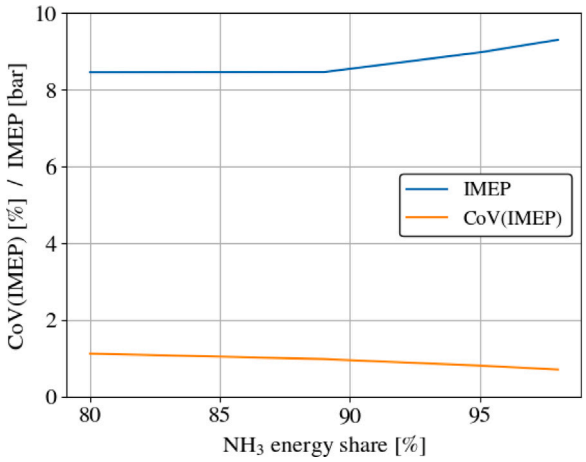

Fig. 9. IMEP [bar] and CoV(IMEP) [%] for different NH_3 energy contributions, with a constant global $\lambda = 1.1$.

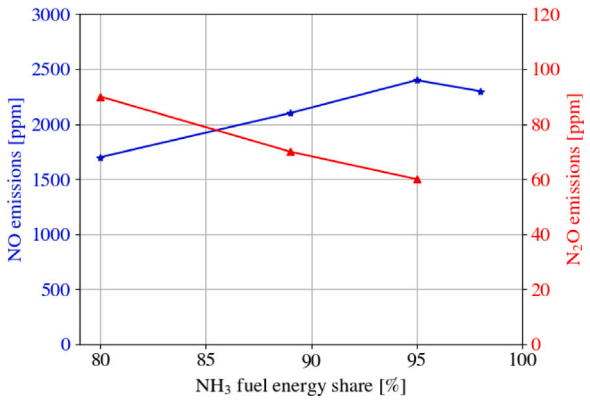

Fig. 10. Emissions of NO and N_2O. The N_2O-measurement at maximum NH_3-level (98.5%) was below the readable range and hence is not shown.

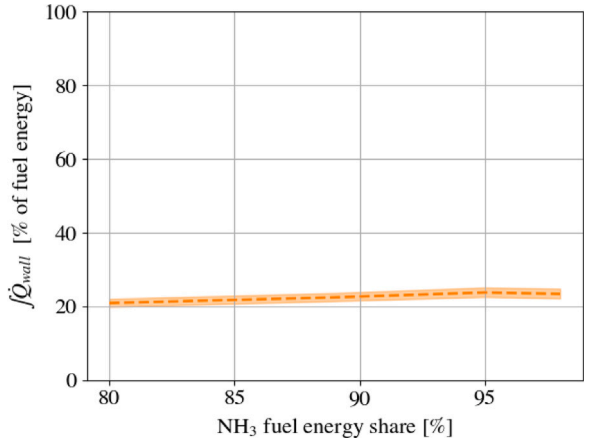

Fig. 11. Sensitivity of the wall heat loss – normalized with fuel-energy – to the residual gas amount f (see Eq. (2.3)). The lower limit is $f = 0.02$, the higher limit is $f = 0.08$, and the stippled line shows the value used for all other results ($f = 0.05$).

The CoV(IMEP) shows that the engine operation was very stable for all the investigated cases, with the higher levels of ammonia-energy reaching less than 1% CoV.

Emissions of NO and nitrous oxide (N_2O) are shown in Fig. 10. The NO-emissions are seen to increase quite linearly with the ammonia energy, which might simply be understood as a larger NO-formation from fuel-bound nitrogen due to the higher amount of ammonia. Thermal NO-formation might also increase due to the longer ignition delays with higher ammonia energy increasing the peak temperature.

N_2O-formation from Thermal DeNOx has been shown to occur mainly from 2 reactions, one dominating at low levels of O_2 (0%–1%) while occurring during high temperatures (Reaction (3.1)) and one dominating at higher levels of O_2 (from 4%) occurring during lower temperatures (Reaction (3.2)) [31,32] .

$$NH + NO \rightleftharpoons N_2O + H \tag{3.1}$$

$$NH_2 + NO_2 \rightleftharpoons N_2O + H_2O \tag{3.2}$$

It has been proposed that in ammonia-burning combustion engines the N_2O-formation mainly occurs from the low-temperature reaction during the expansion stroke as NH_3 from crevices is converted to NH_2 which reacts with NO_2 [6]. This could imply that NH_3 emissions from crevice volumes and N_2O-emissions can be correlated, which is found to be the case in Figs. 6 and 10.

3.1.1. Results discussion

For the presented results the residual gas fraction was assumed to be $f = 0.05$. Higher residual gas fraction increases the temperature at IVC and thus the heat loss through the walls. The sensitivity of the wall heat transfer to f is presented in Fig. 11. The wall heat loss is shown normalized with the fuel energy to present the impact of f on the fraction of fuel energy lost through heat transfer. The range shows f in the range 0.02–0.08. This was chosen since the residual gas fraction is generally very low in CI engines due to the high compression ratios [33,34].

Compared to the case with $f = 0.05$, the heat loss energy fraction – for the investigated range of f – is generally around −5%, or −1.1 percentage points (pp), for $f = 0.02$, and + 5.6%, or + 1.3 pp, for $f = 0.08$.

The integrated heat release (Fig. 5) and the combustion efficiency (Fig. 6) presented earlier matched very well for the cases with 80%–89% ammonia energy. However, 95%–98% NH_3-cases showed higher integrated heat release than the combustion efficiencies. This tendency is also showed in Fig. 12, which shows fuel energy and resulting energy distributions for varying ammonia energy contribution. For 80%–89% ammonia energy, the energy distribution matches the fuel energy very well, while the cases with 95%–98% ammonia energy shows higher total energy distribution than the fuel energy, which clearly breaks the first law of thermodynamics. This is likely partly because the heat loss is over-estimated in these cases, leading to higher heat release, since the heat transfer approximation is probably the greatest source of uncertainty.

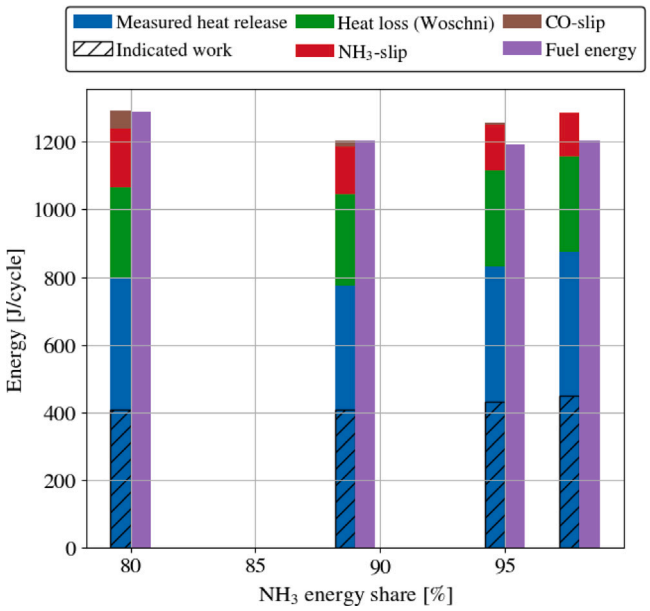

Fig. 12. Distribution of energy.

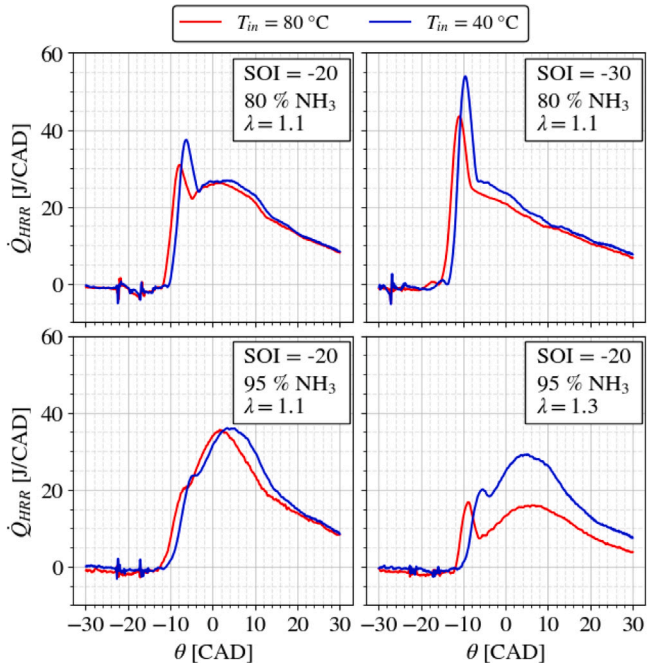

Fig. 13. Heat release rates with intake temperatures at 40 °C and 80 °C with variation of SOI, λ and ammonia energy contribution.

3.2. Intake preheating

Due to the general issues with igniting ammonia and achieving complete combustion, it was expected by the authors that higher intake temperature might result in more complete combustion. For this reason the impact of the intake temperature on the combustion efficiency was studied. Intake ammonia/air-mixture temperatures (T_{in}) of 40 °C and 80 °C were used while varying start of injection (SOI), λ and ammonia energy contribution.

Fig. 13 shows the heat release rates for the studied cases, while Fig. 14 shows the resulting combustion efficiencies.

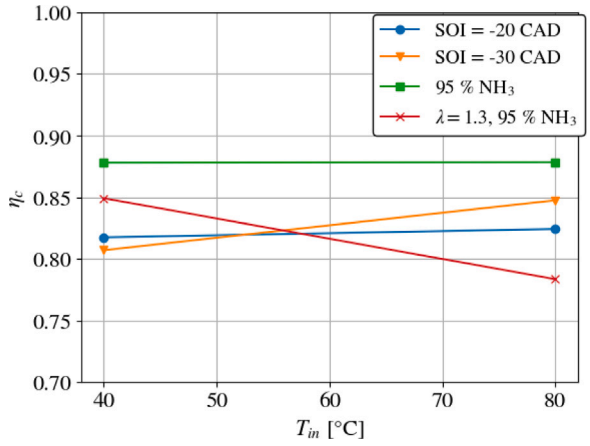

Fig. 14. Combustion efficiency (η_c) vs intake temperature (T_{in}) with parameter variations, related to the heat release rates in Fig. 13.

Generally the heat release rate traces show that intake temperature of 40 °C yield a slightly longer ignition delay than 80 °C, resulting in a higher peak heat release rate due to more pilot fuel mixing time.

Advancing the SOI from 20 to 30 CAD BTDC (the two top graphs in Fig. 13) shows a significantly higher peak heat release rate, most likely also caused by more mixing of the pilot fuel. The later SOI (at 20 CAD BTDC) shows a drop in the heat release rate, effectively dividing the pilot fuel and ammonia combustion phases, while the increased mixing from earlier injection allows the pilot fuel to more effectively start the ammonia combustion, yielding no gap between the two. The related combustion efficiencies in Fig. 14 – denoted as '*SOI = -20 CAD*' and '*SOI = -30 CAD*' – show that increased intake temperature increases improves the combustion with early injection but has only very little impact with the later injection.

Increasing the global air excess ratio λ from 1.1 to 1.3 – i.e. comparing the two bottom graphs in Fig. 13 – shows a gap appear between the pilot fuel and ammonia combustion phases, similarly to the case with 80% ammonia in Fig. 3. This clearly shows that the ammonia is less easily ignited by the pilot fuel due to the leaner ammonia/air mixture and the smaller pilot fuel injection. Furthermore, increasing the intake temperature from 40 °C to 80 °C enhances this gap due to the decreased ignition delay, and very poor ammonia combustion is observed as a result. This is observed in Fig. 14 – denoted 'λ = 1.3, *95% NH_3*' – to be the only case where increased intake temperature decreases the combustion efficiency. The combustion efficiency with 95% NH_3 and λ = 1.1 – denoted '*95% NH_3*' – shows no dependence on the intake temperature.

The IMEP of the results are shown in Table 5 along with the CoV(IMEP) in parentheses. The IMEP is lower with T_{in} = 80 °C than with 40 °C – despite the generally higher combustion efficiency with higher – mainly because equal pilot fuel injection timing was used instead of maximum brake torque (MBT) timing. This results in greater compression stroke work with higher intake temperature due to the earlier ignition. Equal injection timing was chosen to ensure injection into similar conditions of temperature and pressure. Additionally, the higher intake temperature reduces the intake density and thus reduces the fuel injection for a constant λ, also reducing the IMEP. The CoV(IMEP) generally decreases slightly with higher intake temperature, due to slightly higher combustion efficiency.

4. Conclusion

This paper reports tests on a CI-engine using premixed ammonia and direct-injected n-heptane as pilot fuel. By using a GDI nozzle very small amounts of pilot fuel could be used successfully. Energy contribution

Table 5
IMEP [bar] (and CoV(IMEP) [%] in parenthesis) for the results in Figs. 13 and 14. The two top rows correspond to the two top graphs in Fig. 13 and vice versa.

	T_{in}	
	40 °C	80 °C
SOI = −20 CAD	9.3 (1.2%)	8.5 (1.1%)
SOI = −30 CAD	8.9 (1.2%)	7.6 (1.0%)
95% NH_3, λ = 1.1	10.4 (0.8%)	8.7 (0.8%)
95% NH_3, λ = 1.3	8.9 (1.0%)	4.8 (3.3%)

from ammonia was varied in the range 80–98.5% of the injected fuel energy. An important result observed was higher combustion efficiency with increased ammonia energy contribution due to a leaner ammonia–air mixture. Increased values of λ_{NH_3} – the λ-value of the ammonia–air mixture for ammonia combustion – showed a gap in heat release rate between the pilot and ammonia combustion phases due to difficulties in igniting the lean mixture. Lower values of λ_{NH_3} – e.g. from lower total λ or increased ammonia energy contribution – showed no gap between the combustion phases and showed higher peak heat release rate of ammonia. This should allow more heat release close to TDC and thus increase the obtainable indicated efficiency.

The NH_3-emissions were reduced with higher ammonia-content due to higher combustion efficiency, despite the expected increased amount of ammonia in crevice volumes. The N_2O-emissions also decreased with higher ammonia energy, while NO-emissions increased.

The effect of intake temperature on the combustion efficiency was investigated with two values of start of injection (SOI), total λ, and ammonia energy. Increased intake temperature yielded shorter ignition delay for all cases. The cases with SOI = 20 CAD BTDC and λ = 1.1 showed little to no effect of intake temperature on the combustion efficiency. SOI = 30 CAD BTDC showed increased combustion efficiency with higher intake temperature, while λ = 1.3 showed a significantly lower combustion efficiency as the decreased ignition delay showed an increased gap between the combustion phases.

CRediT authorship contribution statement

Niels Førby: Software, Validation, Formal analysis, Data curation, Writing – original draft, Writing – review & editing, Visualization. **Thomas B. Thomsen:** Investigation. **Rasmus F. Cordtz:** Conceptualization, Resources, Project administration. **Frantz Bræstrup:** Investigation, Resources, Data curation. **Jesper Schramm:** Supervision, Funding acquisition.

Declaration of competing interest

The authors declare the following financial interests/personal relationships which may be considered as potential competing interests: Jesper Schramm reports financial support was provided by The Danish Maritime Fund. Jesper Schramm reports financial support was provided by Danish Energy Agency.

Data availability

The experimental data used for the results is freely available in a repository at: https://doi.org/10.11583/DTU.20555586.v2.

Acknowledgments

The authors are grateful for the EUDP and Danish Maritime Fund for financially supporting the research project.

Appendix. The comical corner

Why is it difficult for researchers to concentrate?
- Because they have a-PHD
Why did the company hire Gerhard Woschni?
- Because of his $\dot{Q}_{wall}$ifications

References

[1] Setting the course to low carbon shipping - 2030 outlook/2050 vision. American Bureau of Shipping (ABS); 2019.
[2] Resolution MEPC.304(72). In: Initial IMO strategy on reduction of ghg emissions from ships. International Maritime Organization, (IMO); 2018.
[3] Kim Kyunghwa, et al. A preliminary study on an alternative ship propulsion system fueled by ammonia: Environmental and economic assessments. J Mar Sci Eng 2020;8(3). http://dx.doi.org/10.3390/jmse8030183.
[4] Ammonia as marine fuel. In: NH3 fuel conference. American Bureau of Shipping (ABS); 2020.
[5] Starkman ES, James GE, Newhall HK. Ammonia as a spark engine fuel: Theory and application. SAE Trans 1967;75:765–84. http://dx.doi.org/10.4271/670946.
[6] Westlye Fredrika R, Ivarsson Anders, Schramm Jesper. Experimental investigation of nitrogen based emissions from an ammonia fueled SI-engine. Fuel 2013;111(1):239–47. http://dx.doi.org/10.1016/j.fuel.2013.03.055.
[7] Frigo Stefano, Gentili Roberto. Analysis of the behaviour of a 4-stroke Si engine fuelled with ammonia and hydrogen. Int J Hydrogen Energy 2013;38(3):1607–15. http://dx.doi.org/10.1016/j.ijhydene.2012.10.114.
[8] Lhuillier Charles, et al. Performance and emissions of an ammonia-fueled SI engine with hydrogen enrichment. SAE Technical Paper 2019-24-0137, 2019, http://dx.doi.org/10.4271/2019-24-0137.
[9] Mercier A, et al. Improvement of SI engine combustion with ammonia as fuel: Effect of ammonia dissociation prior to combustion. Fuel Commun 2022;11(March). http://dx.doi.org/10.1016/j.jfueco.2022.100058.
[10] Mørch CS, et al. Ammonia/hydrogen mixtures in an SI-engine: Engine performance and analysis of a proposed fuel system. Fuel 2011;90(2):854–64. http://dx.doi.org/10.1016/j.fuel.2010.09.042.
[11] Stocker TF, et al. Climate change 2013: The physical science basis. Contribution of working group I to the fifth assessment report of the intergovernmental panel on climate change. 2013.
[12] Dimitriou Pavlos, Javaid Rahat. A review of ammonia as a compression ignition engine fuel. Int J Hydrogen Energy 2020;45(11):7098–118. http://dx.doi.org/10.1016/j.ijhydene.2019.12.209.
[13] Gray James T, et al. Ammonia fuel - engine compatibility and combustion. SAE Trans 1967;75:785–807. http://dx.doi.org/10.4271/660156.
[14] Starkman ES, James GE, Newhall HK. Ammonia as a diesel engine fuel: Theory and application. SAE Trans 1968;76:3193–212. http://dx.doi.org/10.4271/670946.
[15] Garabedian Charles G, Johnson John H. The theory of operation of an ammonia burning internal combustion engine. Defense Technical Information Center; 1966.
[16] Kobayashi Hideaki, et al. Science and technology of ammonia combustion. Proc Combust Inst 2019;37(1):109–33. http://dx.doi.org/10.1016/j.proci.2018.09.029.
[17] Reiter Aaron J, Kong Song Charng. Demonstration of compression-ignition engine combustion using ammonia in reducing greenhouse gas emissions. Energy Fuels 2008. http://dx.doi.org/10.1021/ef800140f.
[18] Reiter Aaron J, Kong Song Charng. Combustion and emissions characteristics of compression-ignition engine using dual ammonia-diesel fuel. Fuel 2011;90(1):87–97. http://dx.doi.org/10.1016/j.fuel.2010.07.055.
[19] Frost James, et al. An experimental and modelling study of dual fuel aqueous ammonia and diesel combustion in a single cylinder compression ignition engine. Int J Hydrogen Energy 2021;46(71):35495–510. http://dx.doi.org/10.1016/j.ijhydene.2021.08.089.
[20] Gross Christopher W, Kong Song Charng. Performance characteristics of a compression-ignition engine using direct-injection ammonia-DME mixtures. Fuel 2013;103:1069–79. http://dx.doi.org/10.1016/j.fuel.2012.08.026.
[21] Ryu Kyung Hyun, Zacharakis-Jutz George, Kong Song-Charng. Effects of fuel compositions on diesel engine performance using ammonia-DME mixtures. SAE technical papers 2, 2013, http://dx.doi.org/10.4271/2013-01-1133.
[22] Mounaïm-Rousselle Christine, et al. Performance of ammonia fuel in a spark assisted compression ignition engine. Int J Engine Res 2021;1–12. http://dx.doi.org/10.1177/14680874211038726.
[23] Tat Mustafaa E, Van Gerpen Jon H. The kinematic viscosity of biodiesel and its blends with diesel fuel. JAOCS J Am Oil Chem Soc 1999;76(12):1511–3. http://dx.doi.org/10.1007/s11746-999-0194-0.
[24] Haynes WM. CRC handbook of chemistry and physics. 92nd ed.. CRC Press; 2011.
[25] Dymond JH, Øye HA. Viscosity of selected liquid n-alkanes. J Phys Chem Ref Data 1994;23(May 2014).
[26] European standard EN 590: Automotive fuels - diesel - requirements and test methods. European Committee for Standardization; 2009.

[27] Yanowitz J, et al. Compendium of experimental cetane numbers compendium of experimental cetane numbers. 2017.
[28] Savitzky Abraham, Golay Marcel JE. Smoothing and differentiation of data by simplified least squares procedures. 1964, p. 1627–39. http://dx.doi.org/10.1021/ac60214a047.
[29] Woschni G. A universally applicable equation for the instantaneous heat transfer coefficient in the internal combustion engine. SAE Trans 1967;76:3065–83.
[30] Liu Rui, Ting David SK, Checkel M David. Ammonia as a fuel for SI engine. SAE technical papers 724, 2003, http://dx.doi.org/10.4271/2003-01-3095.
[31] Miller JA, Glarborg P. Modeling the thermal De-NOx process: Closing in on a final solution. Int J Chem Kinet 1999;31(11):757–65. http://dx.doi.org/10.1002/(SICI)1097-4601(1999)31:11<757::AID-JCK1>3.0.CO;2-V.
[32] Kasuya Fumihiko, et al. The thermal DeNOx process: Influence of partial pressures and temperature. Chem Eng Sci 1995;50(9):1455–66. http://dx.doi.org/10.1016/0009-2509(95)00008-S.
[33] Aithal SM. Sensitivity of emissions to uncertainties in residual gas fraction measurements in automotive engines: A numerical study. J Combust 2018. http://dx.doi.org/10.1155/2018/7237849.
[34] Heywood JB. Internal combustion engines fundamentals. McGraw-Hill Inc.; 1988.